35th Annual International Conference of the IEEE EMBS
Osaka, Japan, 3 - 7 July, 2013

Prostate cancer localization by novel magnetic resonance dispersion imaging

M. Mischi, T. Saidov, K. Kompatsiari, M.R.W. Engelbrecht, M. Breeuwer, and H. Wijkstra

Abstract— **Diagnosis and focal treatment of prostate cancer, the most prevalent form of cancer in men, is hampered by the limits of current clinical imaging. Angiogenesis imaging is a promising option for detection and localization of prostate cancer. It can be imaged by dynamic contrast-enhanced (DCE) MRI, assessing microvascular permeability as an indicator for angiogenesis. However, information on microvascular architecture changes associated with angiogenesis is not available. This paper presents a new model enabling the combined assessment of microvascular permeability and architecture. After the intravenous injection of a gadolinium-chelate bolus, time-concentration curves (TCCs) are measured by DCE-MRI at each voxel. According to the convective dispersion equation, the microvascular architecture is reflected in the dispersion coefficient. A solution of this equation is therefore proposed to represent the intravascular blood plasma compartment in the Tofts model. Fitting the resulting model to TCCs measured at each voxel leads to the simultaneous generation of a dispersion and a permeability map. Measurement of an arterial input function is no longer required. Preliminary validation was performed by spatial comparison with the histological results in seven patients referred for radical prostatectomy. Cancer localization by the obtained dispersion maps provided an area under the receiver operating characteristic curve equal to 0.91. None of the standard DCE-MRI parametric maps could outperform this result, motivating towards an extended validation of the method, also aimed at investigating other forms of cancer with pronounced angiogenic development.**

I. INTRODUCTION

In the United States, prostate cancer (PCa) accounts for 29% and 9% of all cancer diagnoses and deaths in males, respectively [1]. The European figures are similar [2]. Despite the availability of effective focal therapies, their timely and efficient use is hampered by a lack of reliable imaging methods for early localization of prostate cancer.

Angiogenesis play a fundamental role in the growth of neoplastic tissue in several forms of cancer, including PCa [3], [4], [5], [6]. It consists of the formation of a dense, irregular network of microvessels, characterized by small, irregular diameters and high tortuosity and permeability (leaky walls). This microvascular network supports cancer growth by carrying nutrients and oxygen.

Many years of research have established angiogenesis as a reliable marker of cancer growth and aggressiveness. Cancer aggressiveness, defined as the risk of developing metastases, has been reported by several authors to correlate well with the immunohistological assessment of the microvascular density (MVD) [7], [4], [8]. Therefore, in the past decades several imaging methods have been introduced aiming at cancer detection through identification of angiogenic processes. These methods seek to quantify the main features characterizing angiogenic microvasculature: microvascular permeability and MVD.

An increased permeability can be detected by dynamic contrast enhanced (DCE) magnetic resonance imaging (MRI). The adopted contrast agents, based on gadolinium chelates, leak across the vascular wall into the extravascular space (interstitium). Quantification of extravascular leakage provides therefore an opportunity to assess vascular permeability and localize the presence of angiogenic processes. Leakage can be assessed by analysis of the transport kinetics of gadolinium by MRI. Assessment of this transport process can be obtained by fitting measured time-concentration curves (TCCs) by the compartmental model introduced by Tofts *et al*. [9]. This model requires knowledge on the arterial input function (AIF), which can be either measured separately [10], or taken from the literature [11], [12]. Fitting the Tofts model to TCCs measured at each voxel results in a local estimate of the volume transfer coefficient between the intravascular and extravascular space. This can be used to generate parametric maps of vascular permeability that permit localizing the presence of angiogenic processes and cancerous tissue.

More challenging is the assessment of changes in the microvascular architecture, such as MVD increase [5]. By using blood pool agents, such as those available for dynamic contrast enhanced ultrasound (DCE-US), many authors have investigated the link between angiogenesis and increased blood perfusion [13], [14], [15]. However, while a lack of vasomotor control and the presence of arteriovenous shunts reduce flow resistance, this can be counterbalanced by small microvessel diameters and increased interstitial pressure due to extravascular leakage [5], [15]. As a result, characterization of the microvascular architecture by perfusion quantification may be unreliable. Recently, a new DCE-US method has been proposed to characterize the microvascular architecture by assessment of the dispersion kinetics of an intravascular contrast agent [16], [17], [18]. Preliminary results for PCa localization are promising and the method seems to overcome the limitations of previous methods based on perfusion quantification.

M. Mischi, T. Saidov, and K. Kompatsiari are with the Electrical Engineering Dept, Eindhoven University of Technology, the Netherlands.

M.R.W. Engelbrecht is with the Radiology Dept, Academic Medical Center, University of Amsterdam, the Netherlands.

M. Breeuwer is with Philips Healthcare, Best, and with the Biomedical Engineering Dept, Eindhoven University of Technology, the Netherlands.

H. Wijkstra is with the Urology Dept, Academic Medical Center, University of Amsterdam, and with the Electrical Engineering Dept, Eindhoven University of Technology, the Netherlands.

978-1-4577-0216-7/13/$26.00 ©2013 IEEE

This paper investigates the feasibility of dispersion imaging by DCE-MRI, here referred to as magnetic resonance dispersion imaging (MRDI). After a peripheral, intravenous injection of a bolus of gadolinium-chelate contrast agent, intravascular dispersion is assessed by fitting a solution of the convective dispersion equation to TCCs measured at each voxel. By doing this, a dispersion parameter, representing the local ratio between contrast convection and dispersion, can be estimated at each voxel. Dispersion, represented by the dispersion coefficient of the convective dispersion equation, is mainly determined by the distribution of contrast transit times due to the multipath trajectories defined by the microvascular architecture [19], [20]. Therefore, dispersion represents a valuable option to characterize the microvascular architecture.

While the convective dispersion model can directly be applied when blood pool agents are used, the presence of extravascular leakage requires separating the intravascular from the extravascular phase. To this end, the dispersion model is combined with the two-compartment Tofts model, representing the intravascular blood plasma compartment. The two-compartment differential equation is then integrated leading to a new model whose parameters permit the assessment of both dispersion and permeability.

The proposed method was evaluated with seven patients diagnosed with prostate cancer and referred for a radical prostatectomy at the Academic Medical Center University of Amsterdam (the Netherlands). After the intravenous injection of a bolus of gadolinium-DPTA, time concentration curves were measured at each voxel and fitted by the proposed model to generate both a permeability and a dispersion map. The proposed method was then evaluated for its capability to distinguish between cancerous and healthy tissue on a voxel basis. The ground truth was represented by the histological results after radical prostatectomy.

II. METHODOLOGY

A. Intravascular model

The kinetics of an intravascular indicator flowing in a microvascular network can be modeled as a Brownian motion process, well described by the convective dispersion equation [19], [21]. In one dimension, z, the convective dispersion equation is given as

$$\frac{dC(z,t)}{dt} = D\frac{d^2C(z,t)}{dz^2} - v\frac{dC(z,t)}{dz}, \tag{1}$$

with $C(z,t)$ being the concentration of the indicator at position z and time t, v being its velocity, and D being the dispersion coefficient. The dispersion coefficient D is affected by concurrent processes, comprising molecular diffusion, flow profile, and transit time distribution due to multipath trajectories of the indicator defined by the microvascular network [20], [21]. In the microvasculature, the latter term is dominant, and dispersion may represent a valuable option to characterize the microvascular architecture [16].

A solution of Eq. (1) is given by the Local Density Random Walk (LDRW) model, which has been extensively used to represent the kinetics of intravascular indicators, such as ultrasound contrast agents, following a bolus injection [22]. More recently, a modified version of the LDRW model has been proposed that enables estimating local parameters, independent of the history of the indicator between the injection and detection site [16]. Its formulation is given as

$$C(t) = \alpha\sqrt{\frac{\kappa}{2\pi(t-t_0)}}e^{\frac{-\kappa(t-t_0-\mu)^2}{2(t-t_0)}}. \tag{2}$$

with t_0 being the theoretical injection time assuming the indicator kinetics to be constant along the entire path between injection and detection site, α being the time integral of $C(t)$, μ being the mean transit time (MTT) of the indicator between injection and detection site, and κ being the estimated intravascular dispersion parameter, $\kappa = v^2/D$, which represents the local ratio between contrast convection (squared velocity v^2) and dispersion (dispersion coefficient D). Equation (2) is a solution of the convective dispersion equation assuming a Gaussian distribution of the contrast bolus in space prior to its passage through each detection voxel [16]. An intravascular dispersion map can be generated by fitting Eq. (2) to TCCs measured at each voxel. This parametric map can be used to detect changes in the microvascular architecture that are due to angiogenic processes.

B. Extravascular model

The LDRW model is directly applicable only for blood pool agents. When extravascular leakage occurs, as with gadolinium-chelate, the intravascular and extravascular dilution phases must be separated. In general, we can define the measured total concentration in a tissue voxel, $C(t)$, as resulting from the contribution of intravascular concentration in blood plasma, $C_p(t)$, and extravascular extracellular concentration in the interstitium, $C_e(t)$, given as

$$C_t(t) = v_pC_p(t) + v_eC_e(t), \tag{3}$$

with v_p being the fractional volume of the intravascular blood plasma and v_e the fractional volume of the interstitium. Assuming the interstitium to be well represented by a single compartment, and assuming the contribution of $C_p(t)$ to $C_t(t)$ to be negligible ($v_p \ll v_e$), the extravasation kinetics can be represented by the model proposed by Tofts *et al.* as

$$C_t(t) = K^{trans}\int_0^t C_p(\tau)e^{-k_{ep}(t-\tau)}d\tau, \tag{4}$$

with $1/K^{trans}$ representing the extravasation time constant and $k_{ep} = K^{trans}/v_e$ representing the back-flow rate from the interstitium to the blood plasma [9]. Both K^{trans} and k_{ep} can be used for assessment of the microvascular permeability. The model in Eq. (4) requires the estimation of $C_p(t)$, i.e., the AIF. This is however well represented by the modified LDRW model in Eq. (2). We can therefore substitute $C_p(t)$ in Eq. (4) by $C(t)$ in Eq. (2). The resulting model, representing both dispersion and extravascular leakage, is given as

$$C_t(t) = \beta\int_{t_0}^{t-t_0}\sqrt{\frac{\kappa}{2\pi(\tau-t_0)}}e^{\frac{-\kappa(\tau-t_0-\mu)^2}{2(\tau-t_0)}}e^{-k_{ep}(t-(\tau-t_0))}d\tau, \tag{5}$$

with $\beta = K^{trans}\alpha$. Fitting Eq. (5) to TCCs measured at each voxel permits the simultaneous estimation of a dispersion map, expressed by κ, and a permeability map, expressed by k_{ep}. Estimation of K^{trans} is hampered by its multiplication by the time integral of Eq. (2), which depends on the flow characteristics in relation to the injected contrast dose (Stewart-Hamilton equation [22]).

C. Model fitting

Curve fitting is performed in order to estimate the five parameters characterizing Eq. (5). To this end, the squared error between the model in Eq. (5) and the measured TCC is minimized. Because of the nonlinear fashion of the adopted model, a nonlinear iterative fitting scheme is adopted. In particular, the search space should be confined in order to reduce the risk of convergence to local minima. To this end, the Trust-Region Reflective method is adopted [23].

A number of search schemes were evaluated by dedicated simulations. For several parameterizations spanning the space representing measured data in patients, 100 TCCs were generated by the proposed model with additional white Gaussian noise, such that the signal-to-noise ratio was similar to that measured in patients (25 dB). The fit error and the fitting time were considered for evaluation of the fitting schemes. Eventually, the selected scheme combines a search grid with the adopted iterative search. In particular, in order to limit the number of parameters to be estimated in the iterative search, the theoretical injection time t_0 is estimated by a grid search with a resolution of 2 s. For each t_0, a Trust-Region Reflective search is performed on the remaining parameters.

For analysis of the acquired data, a TCC must be fitted for each voxel covering the selected ROI. After the parameters k_{ep} and κ are estimated at each voxel, two parametric maps representing permeability and dispersion can be generated. In order to assess the reliability of the estimated parameters, the determination coefficient r^2 of the obtained fit is derived for each voxel; TCC fits with $r^2 < 0.75$ are discarded, as poor fits may provide unreliable parameter estimates. All the analysis is implemented in Matlab (The MathWorks Inc., Natick, MA)

D. Validation

DCE-MRI was performed in seven patients referred for radical prostatectomy at the Academic Medical Center, University of Amsterdam (the Netherlands), by intravenous injection of a 0,1-mmol/Kg bolus of gadolinium-DPTA. All the included patients had signed informed consent. Imaging was performed with a 1.5-T MRI scanner (Magnetom Avanto, Siemens) equipped with an endorectal coil, and using a spoiled gradient recalled sequence and phase oversampling. The adopted sequence parameters were repetition time of 50 ms, echo time of 3.9 ms, flip angle of 70 degrees, slice thickness of 4 mm, and pixel size of 1.67x1.67 mm^2. The resulting time resolution is 2 s for one volume. All data were exported for further analysis in DICOM (Digital Imaging and Communications in Medicine) format.

A preliminary validation was performed by comparison with the histological results. Histological analysis was performed on 4-mm slices where cancerous tissue was marked by a pathologist based on microscopic analysis of cell differentiation (Gleason score) [24]. Only those slices where large regions of interest (ROIs) could be defined to represent a reliable reference for cancerous and healthy tissue were considered. The same ROIs where then overlapped on the corresponding MRI parametric maps in order to assess the ability of the estimated parameters to detect PCa. Tissue classification was then evaluated at voxel level on up to four MRI slices per patient, 19 slices in total. The classification performance of each parameter was evaluated in terms of sensitivity, specificity, and area under the receiver operating characteristic (ROC) curve. All the ROI voxels representing the class of healthy and cancerous tissue were used for this evaluation. The threshold leading to the ROC point that is closest to the top-left corner was considered as the optimal classification threshold for the estimation of sensitivity and specificity. Figure 1 shows an example of parametric dispersion (κ) and permeability (k_{ep}) maps with corresponding histology results.

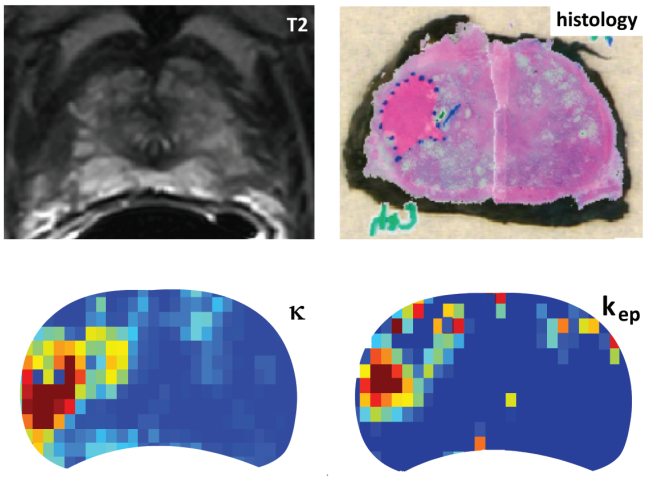

Fig. 1. Example of MRI T2 image with corresponding histology analysis and parametric maps of κ and k_{ep}.

Apart from the estimation of dispersion (κ) and permeability (k_{ep}) by the model in Eq. (5), the assessment of permeability was also performed by fitting the standard Tofts model and estimating its parameters (k_{ep} and K^{trans}). To this end, estimation of the AIF was necessary. We adopted an average AIF based on the literature and modeled with a double exponential, as suggested in [12].

From the fitted model in Eq. (5), the MTT of $C_p(t)$, represented by parameter μ of the modified LDRW model in Eq. (2), was also estimated. The MTT is a measure of intravascular perfusion, and is often adopted for detection of angiogenesis [16]. Additional empiric parameters that are often adopted in the literature were also estimated and adopted for comparison. These are the wash-in rate, the peak enhancement, slope_50, and wash-out rate [25].

III. RESULTS

Only curve fits with $r^2 > 0.75$ were used to evaluate the classification performance of the method. The discarded curves were however only 8% of all the measured curves, confirming an accurate fitting performance.

All the classification results are reported in Table I. Classification is evaluated at a voxel level in terms of sensitivity, specificity, and ROC curve area.

TABLE I
CLASSIFICATION RESULTS.

Parameter	Sensitivity (%)	Specificity (%)	ROC area
κ (MRDI)	82.6	89.5	0.91
k_{ep} (MRDI)	58.0	80.9	0.72
MTT (MRDI)	61.2	43.7	0.52
k_{ep} (Tofts)	85.3	85.3	0.91
K^{trans} (Tofts)	79.7	83.1	0.88
wash-in rate	76.7	76.1	0.81
wash-out rate	80.5	85.7	0.88
slope_50	75.3	76.1	0.82
peak enhancement	75.1	82.6	0.82

IV. DISCUSSION AND CONCLUSIONS

A new DCE-MRI method is proposed for the characterization of microvascular architectures by assessment of contrast intravascular dispersion, without need for a separate AIF estimation. The results are promising and motivate further research on this new option for PCa localization.

The use of multi-parametric MRI, usually combining standard T2, permeability, and diffusion-weighted imaging, is recently gaining attention in order to improve PCa diagnosis. Also in this context, MRDI can provide a valuable contribution by integration of a dispersion parameter characterizing the microvascular architecture.

The proposed dispersion maps show accurate classification of cancer tissue as compared to histology. Classification by the simultaneously-estimated permeability parameter k_{ep} is less accurate. The reason can possibly reside in a dependency between the model parameters. In future work, model sensitivity analysis will be carried out to investigate this issue.

Histology was considered as the ground truth for validation. However, while histology grading is based on the degree of cell differentiation (Gleason score) [24], dispersion characterizes the microvascular architecture. In the future, comparison with immunohistological MVD maps will therefore be considered.

In general, although the proposed preliminary validation focuses on PCa diagnosis, the proposed method is applicable for diagnosis of any form of cancer where angiogenesis and neovascularization play an important role.

REFERENCES

[1] A. C. Society, "Cancer facts & figures 2012," *Atlanta: American Cancer Society*, 2012.

[2] J. Ferlay, P. Autier, M. Boniol, M. Heanue, M. Colombet, and P. Boyle, "Estimates of the cancer incidence and mortality in europe in 2006," *Ann. Oncol.*, vol. 18, pp. 581–592, 2007.

[3] J. Folkman, "Induction of angiogenesis during transition from hyperplasia to neoplasya," *Nature*, vol. 339, pp. 58–61, 1989.

[4] M. Brawer, "Quantitative microvessel density. a staging and prognostic marker for human prostatic carcinoma," *Cancer*, vol. 78, no. 2, pp. 345–349, 1996.

[5] G. Russo, M. Mischi, W. Scheepens, J. De la Rosette, and H. Wijkstra, "Angiogenesis in prostate cancer: onset, progression and imaging," *BJU International*, vol. 110, pp. 794–808, 2012.

[6] N. Weidner, P. R. Carroll, J. Flax, W. Blumenfeld, and J. Folkman, "Tumor angiogenesis correlates with metastasis in invasive prostate carcinoma," *Am. J. Pathology*, vol. 143, no. 2, pp. 401–409, 1993.

[7] S. Bigler, R. Deering, and M. Brawer, "Comparison of microscopic vascularity in benign and malignant prostate tissue," *Hum. Pathol.*, vol. 24, no. 2, pp. 220–226, 1993.

[8] S. Fox, G. Gasparini, and A. Harris, "Angiogenesis: Pathological, prognostic, and growth-factor pathways and their link to trial design and anticancer drugs," *Lancet Oncol.*, vol. 2, no. 5, pp. 278–289, 2001.

[9] P. Tofts, G. Brix, D. Buckley, and J. Evelhoch, "Estimating kinetic parameters from dynamic contrast-enhanced T1-weighted MRI of a diffusable tracer: Standardized quantities and symbols," *Journal of Magnetic Resonance Imaging*, vol. 10, pp. 223–232, 1999.

[10] E. Vonken, M. van Osch, C. Bakker, and M. Viergever, "Measurement of cerebral perfusion with dual-echo multi-slice quantitative dynamic susceptibility contrast MRI," *J Magnetic Resonance Imaging*, vol. 10, no. 2, pp. 109–117, 1999.

[11] G. Parker, C. Roberts, A. Macdonald, G. Buonaccorsi, S. Cheung, D. Buckley, A. Jackson, and Y. Watson, "Experimentally-derived functional form for a population-averaged high-temporal-resolution arterial input function for dynamic contrast-enhanced MRI," *Magn. Reson. Med.*, vol. 56, pp. 993–1000, 2006.

[12] P. Tofts and A. Kermode, "Measurement of the blood-brain barrier permeability and leakage space using dynamic MR imaging. I. Fundamental concepts," *Magn. Reson. Med.*, vol. 17, pp. 357–367, 1991.

[13] N. Elie, A. Kaliski, P. Péronneau, P. Opolon, A. Roche, and N. Lassau, "Methodology for quantifying interactions between perfusion evaluated by DCE-US and hypoxia throughout tumor growth," *Ultrasound in Med. and Biol.*, vol. 33, no. 4, pp. 549–560, 2007.

[14] R. J. Eckersley, J. P. Sedelaar, M. J. K. Blomley, H. Wijkstra, N. M. deSouza, D. O. Cosgrove, and J. J. M. C. H. de la Rosette, "Quantitative microbubble enhanced transrectal ultrasound as a tool for monitoring hormonal treatment of prostate carcinoma," *Prostate*, vol. 51, pp. 256–267, 2002.

[15] D. Cosgrove, "Angiogenesis imaging - ultrasound," *The British Journal of Radiology*, vol. 76, pp. S43–S49, 2003.

[16] M. Kuenen, M. Mischi, and H. Wijkstra, "Contrast ultrasound diffusion imaging for localization of prostate cancer," *IEEE Trans. on Medical Imaging*, vol. 30, pp. 1493–1502, 2011.

[17] M. Mischi, M. Kuenen, and H. Wijkstra, "Angiogenesis imaging by spatiotemporal analysis of ultrasound-contrast-agent dispersion kinetics," *IEEE Trans. on Ultras., Ferro., and Freq. Contr*, vol. 59, no. 4, pp. 621–629, 2012.

[18] M. Smeenge, M. Mischi, M. Laguna Pes, J. De la Rosette, and H. Wijkstra, "Novel contrast-enhanced ultrasound imaging in prostate cancer," *World J Urology*, vol. 29, no. 5, pp. 581–587, 2011.

[19] D. de Wiest, "Flow through porous media," *New York: Academic Press*, 1969.

[20] G. I. Taylor, "Dispersion of soluble matter in solvent flowing slowly through a tube," *Proc R Soc Lond*, vol. 219, no. 1137, pp. 186–203, 1953.

[21] C. W. Sheppard, *Basic principles of the tracer method*. New York: John Wiley and Sons, 1962.

[22] M. Mischi, "Contrast echocardiography for cardiac quantifications," *ISBN 90-386-16-13-9, Eindhoven University of Technology*, 2004. Online: http://www.bmdresearch.com/db/files/23.pdf.

[23] T. Coleman and Y. Li, "An interior, trust region approach for nonlinear minimization subject to bounds," *SIAM Journal on Optimization*, vol. 6, pp. 418–445, 1996.

[24] D. F. Gleason and G. T. Mellinger, "Prediction of prognosis for prostatic adenocarcinoma by combined histological grading and clinical staging," *J Urol*, vol. 111, no. 1, pp. 58–64, 1974.

[25] A. Padhani, "Dynamic contrast-enhanced MRI in clinical oncology: current status and future directions," *J. Magn. Reson. Imaging*, vol. 16, no. 4, pp. 407–422, 2002.